RSC Advances

ROYAL SOCIETY OF CHEMISTRY

www.rsc.org/advances

Journal Name

ARTICLE TYPE

Cite this: DOI: 10.1039/xxxxxxxxxx

Solvent Tunable Photophysics of Acridone: A Quantum Chemical Perspective

Vidisha Rai-Constapel and Christel M. Marian*

Received Date
Accepted Date

DOI: 10.1039/xxxxxxxxxx

www.rsc.org/journalname

High-level electronic structure methods and quantum chemistry programs have been employed for a thorough investigation of the photophysics of acridone in isolated and solvated states. A kaleidoscope of photophysical behavior results by varying the medium in which acridone finds itself. With the computed intersystem crossing rate constants of the order of $10^{11}s^{-1}$ in vacuum, the photoexcited species acts as an effective triplet sensitizer. In polar, aprotic media, the radiationless decay processes for the photoexcited singlet state are still predominant, however, a delayed fluorescence may also be observed. Such delayed fluorescence comes into play due to the near degeneracy of the $^1(\pi_H\pi_L^*)$ and $^3(n_O\pi_L^*)$ electronic states in such a solvent. As the polarity, as well as the proticity of the solvent increases, the energy shifts experienced by the involved electronic states cause the photoexcited molecule to relax primarily via fluorescence emission to the ground state with a rate constant of the order of about 10^7s^{-1}. In such solvents, acridone is a good fluorescence marker. Hence, tuning the polarity and proticity of the solvent should turn acridone into a dark (triplet formation) or a bright (fluorescence) sensitizer.

1 Introduction

Acridone (AC) belongs to the xanthone group of aromatic ketones (see Fig.1). Along with its derivatives, AC is commonly used in pharmaceutical applications.[1]

A review article by Zhao et al. mentions the possible use of AC as triplet sensitizer in a triplet-triplet annihilation upconversion scheme based on the fact that intersystem crossing (ISC) from the singlet to the triplet state in photoexcited AC is feasible without the involvement of any heavy atoms, the ISC being promoted via $n \rightarrow \pi^*$ type transitions.[2] The triplet sensitizing properties of AC have also been been exploited for exciting Eu^{3+} in a complex used as a luminescent marker in biological applications.[3] AC itself is also applied as a fluorescent probe for DNA labeling.[4] The solvent dependent luminescence of AC has been made use of to design a pair of donor-accpetor-donor triads with a potential for application as organic semi-conductors.[5]

Whether AC acts as a triplet sensitizer or as a fluorescent marker, depends upon the excited-state energy landscape. This landscape, in turn, varies with the type of medium (or the absence of it!) surrounding the molecule. Though experimental studies regarding the various applications of AC are numerous, an extensive theoretical analysis of its photophysics was not found in the literature. Previous theoretical works on the related molecules xanthone (X) and thioxanthone (TX), have established the importance of theory in order to gain a better insight and understanding of the excited-state processes.[6–9] This paper extends such an analysis to AC and presents a detailed quantum chemical study of this molecule in vacuum, as well as four solvents, namely, chloroform, acetonitrile (AcN), methanol (MeOH) and water.

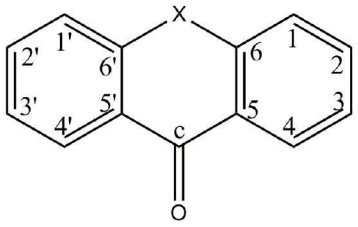

Fig. 1 Molecular structure of the xanthone family of molecules: thioxanthone (X=S), xanthone (X=O) and acridone (X=NH)

*Institute of Theoretical and Computational Chemistry, Heinrich Heine University Düsseldorf, Universitätsstr. 1, D-40225 Düsseldorf, Germany; E-mail: Christel.Marian@hhu.de

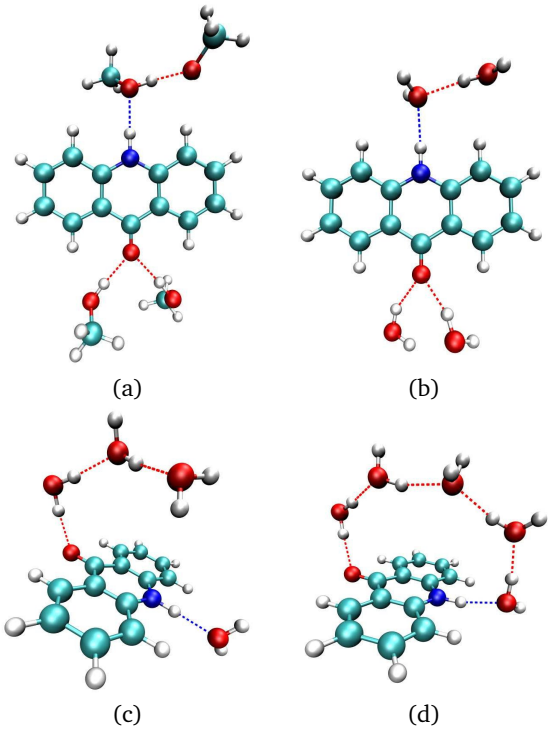

Fig. 2 Micro Solvation Models

2 Computational Details

Detailed information about the basis sets, functionals and methods used for the geometry optimization of the ground and excited states of isolated AC is the same as that used for thioxanthone (TX) and xanthone (X) and may be found in our previous works.[6,7] Geometry optimization of the ground state was carried out at the level of density functional theory (DFT) using the B3LYP functional[10,11] and the standard TZVP basis set[12] as implemented in the TURBOMOLE [13] program package. For the optimization of the electronically excited state geometries time-dependent DFT[14] (TDDFT) was employed. To ensure that the resulting geometries correspond to true minima of the potential energy surface (PES), harmonic vibrational frequencies were calculated numerically with the program SNF[15].

The conductor-like screening model (COSMO) implemented was used to take account of the electrostatic interaction of AC with the solvent.[16,17] The effect of specific bonding with solvent molecules was taken account of via micro-solvation. To this purpose, explicit solvent molecules were placed at appropriate hydrogen bondig sites of AC and the whole system was enveloped by the implicit solvation model COSMO (see Fig.2).

Single-point calculations at the optimized structures were carried out using the DFT/MRCI method in order to obtain the vertical excitation energies, dipole moments and oscillator strengths.[18] For the isolated molecule, the calculations were carried out in the C_{2v} symmetry. Due to technical reasons, DFT/MRCI calculations involving COSMO had to be carried out in the C_1 symmetry. In the DFT/MRCI step, the solvent effect is incorporated solely by adding the solute-solvent interaction terms to the Fock matrix of the reference state, i.e., electronic relaxation effects and the costs required for the polarization of the solvent are not accounted for.[19] The ISC rate constants were calculated in the Condon approximation which requires the electronic spin-orbit coupling matrix elements and the vibrational overlaps. The program SPOCK developed in our group was employed to determine the spin-orbit matrix elements (SOMEs) between the correlated DFT/MRCI wavefunctions.[20,21] Recently, a time-dependent method for computing ISC rate constants has been developed in our laboratory. This method can also take account of temperature effects on the rate constants if desired.[22,23] Computation of the ISC rate constants in this work is based on this program.

A qualitative analysis of the photophysical processes occuring after the photoexcitation has been carried out by following the linearly interpolated path (LIP) between the minima of the electronic states involved. At each of the chosen points along the LIP, a single-point DFT/MRCI calculation was carried out to determine the energy profile of the singlet and triplet excited electronic states.

3 Vertical Excitation Spectra: Vacuum and Solvent

The energetic positions of the electronic states after photoexcitation at the Franck-Condon (FC) point gives a first view of the energy landscape of the species under various conditions. In the following, the vertical excitation spectra of the isolated and solvated AC are presented. Table1 lists the vertical excitation energies of the low-lying electronic states at the FC point for various cases along with the corresponding data available in literature. The present computational values show an overall good agreement with those experimentally reported.

Vacuum. The equilibrium geometry of the ground state (S_0) of isolated AC is C_{2v} symmetric. We found this planar structure to be marginally more stable than the C_s symmetric one, which has been refered to by Boużyk et al. as being the equilibrium geometry of the ground state.[26] In vacuum, the first two singlet excited states, $S(n_O\pi_L^*)$ and the bright $S(\pi_H\pi_L^*)$, are nearly degenerate, with the former lying about 0.04 eV lower in energy. The frontier orbitals involved in these electronic excitations are depicted in Fig.3. Mitsui et al. measured the fluorescence excitation spectrum of AC under jet-cooled conditions.[27] They found the $^1(\pi\pi^*)$ origin band at 3.38 eV which compares well with our calculated value of 3.50 eV (see Table1). The lowest-lying triplet state in the energy spectrum, at 2.94 eV, is the one with $\pi_H\pi_L^*$ character. About 0.06 eV above this state lies the $T(n_O\pi_L^*)$ state. The

Table 1 Vertical singlet and triplet excitation energies ΔE [eV] in vacuum and solvent at the respective ground state minima of AC.

State		Electronic structure[a]	ΔE						
			Vacuum	$CHCl_3$	AcN	MeOH	Water(b)	Water(c)	Water(d)
S_0	1^1A_1	(94.7) ground state	0.00	0.00	0.00	0.00	0.00	0.00	0.00
S_1	1^1A_2	(75.4) $n_O \rightarrow \pi_L^*$	3.46	3.67	3.75	3.97	4.11	3.85	3.87
			0.00[b]						
S_2	2^1A_1	(80.1) $\pi_H \rightarrow \pi_L^*$	3.50 (3.38[c])	3.43	3.40 (3.31[d])	3.31 (3.27[e])	3.32 (3.23[f])	3.33	3.33
			0.14						
T_1	1^3A_1	(83.7) $\pi_H \rightarrow \pi_L^*$	2.94 (2.90[c])	2.85	2.80	2.65	2.68	2.71	2.69
			0.00						
T_2	1^3A_2	(76.6) $n_O \rightarrow \pi_L^*$	3.30	3.53	3.61	3.85	4.00	3.72	3.73
			0.00						
T_3	1^3B_2	(31.7) $\pi_H \rightarrow \pi_{L+1}^*$, (19.1) $\pi_{H-1} \rightarrow \pi_L^*$	3.58	3.58	3.58	3.54	3.55	3.56	3.56
		(12.4) $\pi_{H-3} \rightarrow \pi_L^*$, (11.1) $\pi_{H-2} \rightarrow \pi_{L+2}^*$	*0.00*						
T_4	2^3A_1	(57.8) $\pi_{H-2} \rightarrow \pi_L^*$, (12.0) $\pi_{H-3} \rightarrow \pi_{L+2}^*$	3.59	3.61	3.61	3.64	3.63	3.62	3.62
			0.01						

[a] The characterization of the electronic states is based on the gas-phase results.
[b] The oscillator strengths are italicized.
[c] AC monomer, band origin [24]
[d] AC in AcN, band maximum [25]
[e] AC in MeOH, band maximum [25]
[f] AC in water, band maximum [25]

energetic positions of these two triplet states, namely, $T(\pi_H\pi_L^*)$ at 2.90 eV and $T(n_O\pi_L^*)$ at 3.13 eV, deduced by Mitsui et al. based on their study of the bare AC, are in near perfect agreement with our results (compare Table1).[24] The other higher-lying triplet states have a multiconfigurational $\pi\pi^*$ character and are located slightly higher in energy than the bright singlet excited state.

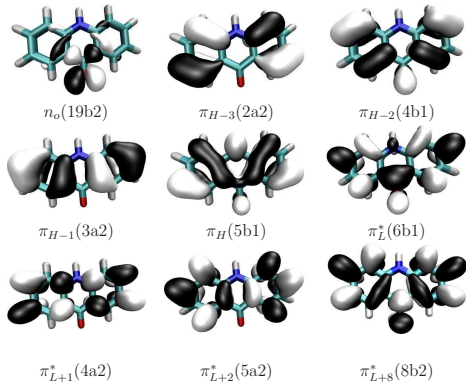

Fig. 3 Frontier orbitals at the optimized ground-state (S_0) geometry (Isovalue=0.02)

Chloroform. In order to study the effect of increasing the polarity of the surrounding medium, we put AC in $CHCl_3$ which has a dielectric constant, ε, of 4.81. As in vacuum, the C_{2v} symmetric character of the ground state is preserved. Already for this slightly polar solvent, the $(n_O\pi_L^*)$ states experience a significant blue shift of about 0.21 eV (see Table1). The red shift experienced by the $S(\pi_H\pi_L^*)$ state being only 0.07 eV, this state now lies 0.24 eV below the corresponding $(n_O\pi_L^*)$ state in the vertical excitation spectrum. The $T(\pi_H\pi_L^*)$ is also slightly red shifted and lies at 2.85 eV at the FC point.

Acetonitrile. Next we put AC in AcN medium. AcN is a polar (ε=36), non-protic solvent. The ground state remains C_{2v} symmetric. The $S(n_O\pi_L^*)$ is blue shifted by 0.29 eV in AcN, hence, now lying 0.35 eV above the $S(\pi_H\pi_L^*)$ state in the vertical excitation spectrum. The energetic position of the $S(\pi_H\pi_L^*)$ at the FC point has been experimentally reported to be 3.31 eV, in very good agreement with our computed value of 3.40 eV.[25] Corresponding shifts are observed in the triplet manifold with the $T(n_O\pi_L^*)$ state blue shifted by 0.31 eV, whereas the $T(\pi_H\pi_L^*)$ state is red shifted by 0.14 eV, thus lying at 2.80 eV in the vertical excitation spectrum. The higher-lying multiconfigurational triplet states experience only minimal red shifts (see Table1).

Methanol. In our previous studies of X and TX we have already discussed the importance of taking account of hydrogen bonding for the photophysics in polar, protic solvents.[6,8] To highlight the effect of specific bond formation, AC was studied in MeOH (ε=33) which is nearly as polar as AcN, may, however, form H-bonds with AC (see Fig.2). In contrast to X and TX, AC forms specific bonds at two sites, namely, the oxygen of the carbonyl group and the hydrogen at the NH group. Due to H-bond formation, the blue shift experienced by the $n_O\pi_L^*$ states, as well as the red shift undergone by the $\pi_H\pi_L^*$ states is about twice as large as that in AcN (see Table1). The bright $S(\pi_H\pi_L^*)$ is about 3.31 eV above the S_0 state. Siegmund and Bending report the peak for absorption to this state at about 3.27 eV, which supports our result.[25]

Water. The energy gap between the states of $n_O\pi_L^*$ and $\pi_H\pi_L^*$ characters should be further enhanced in water (ε=78), since this is a very polar solvent. We computed three different specific bond models in aqueous solution (see Fig.2). In the two models (c) and (d) shown in Fig.2 we placed two explicit water molecules so as to form H-bonds at the NH and CO sites and further water molecules so as to allow for the formation of a bridge-like structure connecting the NH and CO ends of AC. In the case of TX, our computations showed that the number of H-bonds formed at the H-bonding site may significantly influence the photophysics in a particular solvent.[8] Similar observation is made here. In the bridged models, the oxygen of the carbonyl group forms one H-bond with the explicit solvent molecule and the hypsochromic shift of the $n_O\pi_L^*$ states is somewhere between that calculated in AcN and MeOH media (see Table1). As can be seen from Table1, both the four and five explicit solvent models, water(c) and water(d), respectively, have nearly identical vertical excitation energies for the various electronic states, indicating that the H-bonding effect is saturated. Further addition of explicit solvent molecules along the chain would not cause any significant variation. In their paper regarding microscopic solvation effects, Mitsui et al. come to the same conclusion.[24] A look at the vertical excitation energies of the water model (b) shows that the blue shift is enhanced as compared to that in the bridged models, indicating that the number of H-bonds formed at the carbonyl group should indeed be taken account of. Hence, in the following, only the model (b) has been chosen for further discussion of AC in aqueous medium.

For the explicit solvent model (b) (see Fig.2), the blue shift of the $n_O\pi_L^*$ is enhanced as two H-bonds are formed at the carbonyl oxygen. We observe that the red shift experienced by the $\pi_H\pi_L^*$ states remains pretty much the same irrelevant of the explicit solvation model. The major absorption band corresponding to $S_0 \rightarrow S(\pi_H\pi_L^*)$ transition at 3.23 eV observed by Siegmund et al. for AC in aqueous solution agrees well with the calculated vertical excitation energy of 3.32 eV for the bright singlet $S(\pi_H\pi_L^*)$ state at the S_0 minimum. As in AcN and MeOH, the multiconfigurational triplet $\pi\pi^*$ states are not much influenced by the solvent.

4 Adiabatic Minima and Photophysics

After photoexcitation from the ground state to an electronically excited state, the layout of the adiabatic minima of the various excited states in the singlet and triplet manifold governs the photophysically available relaxation channels. To this purpose the adiabatic minima of the relevant electronic states were determined. Table2 lists the calculated and estimated adiabatic energies of the excited states. The estimated adiabatic energies in solvents are calculated by applying the solvent shift experienced by the respective states at the FC point in the various media to the adiabatic energies of these states determined in vacuum. The LIPs between the various adiabatic minima give a good qualitative view of the photophysics of the excited molecule.

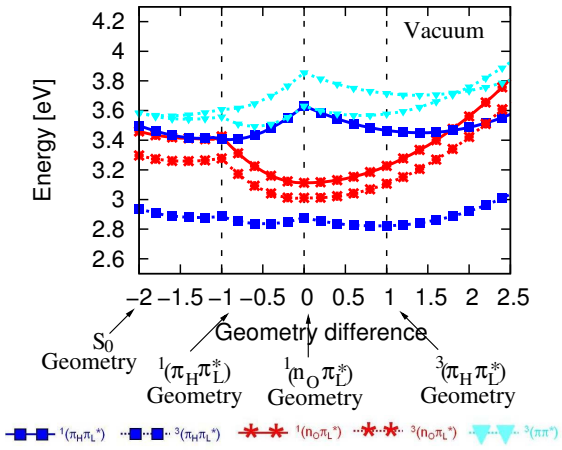

Fig. 4 DFT/MRCI excitation energy profiles in vacuum.

Vacuum. The lowest-lying singlet and triplet excited states of AC are computed to have C_{2v} symmetric minimum structures in the gas phase. A photoexcitation at the FC point results in the population of the bright singlet excited state with $\pi_H\pi_L^*$ character. Fig.4 shows the LIP between the minima of the initially photoexcited state and the relevant electronic states. The two photophysically relevant singlet states, namely, $S(\pi_H\pi_L^*)$ and $S(n_O\pi_L^*)$, are isoenergetic at this minimum. The two corresponding triplets lie energetically below the bright singlet state. Whether the $S(\pi_H\pi_L^*)$ relaxes radiatively (fluorescence to the ground state) or nonradiatively (internal conversion (IC) to the $S(n_O\pi_L^*)$ and ISC to the lower- lying triplets) will depend upon the rate constants of the various processes. In the following we discuss this in detail.

The computed rate constant for radiative emission to the ground state is $k_f = 6.4\times10^7$ s^{-1}. However, since the two singlets ($S(\pi_H\pi_L^*)$ and $S(n_O\pi_L^*)$) are isoenergetic at the $S(\pi_H\pi_L^*)$ minimum (see Fig.4), the rate constant for the radiationless IC process is expected to be larger by some orders of magnitudes as compared to k_f. Besides IC, the $S(\pi_H\pi_L^*) \rightsquigarrow T(n_O\pi_L^*)$ and $S(n_O\pi_L^*) \rightsquigarrow T(\pi_H\pi_L^*)$ ISC channels are also feasible. The SOMEs for the two channels are i19.40 cm^{-1} and i42.38 cm^{-1}, respectively. Both the channels are El-Sayed allowed channels, so why do the SOMEs for the two channels differ that much?

In order to understand this we took a closer look at the configuration of the involved electronic states at the minima of the two singlet states. We find that, at the adiabatic minimum of the $S(\pi_H\pi_L^*)$ state, this state comprises 81% of $\pi_H \rightarrow \pi_L^*$ electronic transition. The $n_O \rightarrow \pi_L^*$ transition contributes 77% to the $T(n_O\pi_L^*)$ configuration. Hence, both the states are highly pure. Now we go to the adiabatic minimum of the $S(n_O\pi_L^*)$ and investigate the composition of this and the $T(\pi_H\pi_L^*)$ state. The $S(n_O\pi_L^*)$ is nearly

Table 2 Adiabatic ΔE_{adia} and estimated ΔE_{est} singlet and triplet DFT/MRCI excitation energies (in [eV]) of low-lying excited states of AC.

	vacuum	$CHCl_3$	AcN		MeOH		water	
Geometry	ΔE_{adia}	ΔE_{est}	ΔE_{adia}	ΔE_{est}	ΔE_{adia}	ΔE_{est}	ΔE_{adia}	ΔE_{est}
$^1(n_O\pi_L^*)$	3.11	3.32	3.61	3.40	–	3.62	–	3.75
$^1(\pi_H\pi_L^*)$	3.41	3.34	3.30	3.31	3.17	3.22	3.20	3.23
$^3(\pi_H\pi_L^*)$	2.82	2.73	2.71	2.68	–	2.53	2.58	2.56
$^3(n_O\pi_L^*)$	3.01	3.30	3.50	3.31	–	3.56	–	3.71
$^3(\pi\pi^*)^a$	3.55	3.55	–	3.55	–	3.51	–	3.52

[a] multiconfigurational triplet states, see Table1.

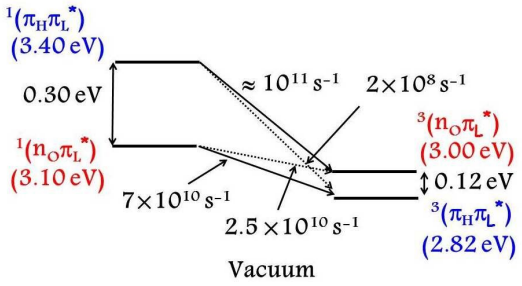

Fig. 5 The feasible ISC channels in photoexcited AC in vacuum.

pure with 77% contribution from the $n_O \rightarrow \pi_L^*$ electronic transition. However, the $T(\pi_H\pi_L^*)$ state shows a mixed configuration character. We find a 70% contribution from the $\pi_H \rightarrow \pi_L^*$ and a 15% contribution from the $\pi_{H-1} \rightarrow \pi_L^*$ electronic transition for the $T(\pi_H\pi_L^*)$ state at the $S(n_O\pi_L^*)$ minimum. Looking at the involved orbitals (see Fig.3), we see that the charge transfer character of the $S(n_O\pi_L^*) \rightsquigarrow T(\pi_H\pi_L^*)$ transition is enhanced due to the involvment of the π_{H-1} orbital. In the $\pi_{H-1} \rightarrow \pi_L^*$ transition, a marked increase in the elctron density at the carbonyl group takes place, explaining the larger SOME for this process.

The scheme in Fig.5 summarises the various ISC channels available in vacuum. Due to the energetically close vicinity of the $(\pi_H\pi_L^*)$ and $(n_O\pi_L^*)$ states, we expect the El-Sayed forbidden channels to be also feasible in addition to the allowed direct ISC path. A rate constant of $k_{ISC} \approx 10^{11}$ s^{-1} is computed for the $S(\pi_H\pi_L^*) \rightsquigarrow T(n_O\pi_L^*)$ El-Sayed allowed relaxation path. The rate constant of the vibronically allowed $S(\pi_H\pi_L^*) \rightsquigarrow T(\pi_H\pi_L^*)$ channel is about 3 orders of magnitude smaller and may, hence, safely be ignored in the photophyiscal discussion. The dark $S(n_O\pi_L^*)$ state is populated via IC from the $S(\pi_H\pi_L^*)$ state. The rate constants for the El-Sayed allowed and forbidden ISC processes arising from this dark state are computed to be of the same order of magnitude,namely $\approx 10^{10}$s^{-1}, with the direct channel being slighlty faster than the vibronically induced one.

Mitsui et. al conclude in their paper that in isolated AC an efficient formation of the triplet state occurs after photoexcitation.[24] Our results agree and undermine the statement. They further deduce that the dominant nonradiative deactivating channel is $S(\pi\pi^*) \rightsquigarrow T(n\pi*)$ followed by $T(n\pi*) \rightsquigarrow T(\pi\pi^*)$. Here we propose an alternative deactivation channel, namely, $S(\pi_H\pi_L^*) \rightsquigarrow S(n_O\pi_L^*)$ followed by $S(n_O\pi_L^*) \rightsquigarrow T(\pi_H\pi_L^*)$. As mentioned above, the isoenergetic position of the involved singlet states at the minimum of the bright state and the energetically lower-lying adiabatic minimum of the dark state lend credibility to the deactiviation channel proposed by us.

Also, surprisingly, the SOME of ≈ 40cm^{-1} reported by Mitsui et al. for the $S(\pi\pi^*) \rightsquigarrow T(n\pi*)$ channel compares well with that computed by us for the $S(n_O\pi_L^*) \rightsquigarrow T(\pi_H\pi_L^*)$ deactivation process.[24]

Chloroform. As already hinted by the energy shifts at the FC point, the adiabatic minima of the $(n_O\pi_L^*)$ and $(\pi_H\pi_L^*)$ states are affected to varying extents by the polarity of the solvent. The LIPs shown in Fig.6 provide an overview of the various possibilities which the photoexcited AC has at it's disposal for relaxation purposes. As compared to vacuum, it is seen that the isoenergeticity of the involved singlet states at the adiabatic minimum of the $S(\pi_H\pi_L^*)$ is lifted. However, IC from the bright $S(\pi_H\pi_L^*)$ to the dark $S(n_O\pi_L^*)$ state remains the predominant radiationless relaxation channel. This is due to the fact that the adiabatic minima of the two states are only 0.02 eV apart in $CHCl_3$, with $S(n_O\pi_L^*)$ minimum lying below that of the $S(\pi_H\pi_L^*)$ state. The $S(n_O\pi_L^*)$ state may, in turn, relax radiationlessly via ISC to the $T(\pi_H\pi_L^*)$ state. The rate constant for the $S(n_O\pi_L^*) \rightsquigarrow T(\pi_H\pi_L^*)$ channel is computed to be 1.8×10^9s^{-1}. Based on the fact that the minima of the sinlget states are so close to each other, a reverse IC from the $S(n_O\pi_L^*)$ could repopulate the $S(\pi_H\pi_L^*)$ state.

The ISC channel $S(\pi_H\pi_L^*) \rightsquigarrow T(n_O\pi_L^*)$ with a computed rate constant of $\approx 10^{10}$s^{-1} is the competing channel to the IC process mentioned above. The adiabatic minima of these two states lie only 0.04 eV apart,however, the reverse ISC process $T(n_O\pi_L^*) \rightsquigarrow S(\pi_H\pi_L^*)$ with a rate constant of $k_{ReISC} = 4.1\times10^8$s^{-1} is about an order of magnitude slower. Summarizing, the radiationless processes dominate the photophysics in the moderately polar solvent, quenching the radiative channels.

Acetonitrile. In AcN the stabilization of the $(\pi_H\pi_L^*)$ states and the destabilization of the $(n_O\pi_L^*)$ states leads to a larger energetic separation of $^{1,3}(n_O\pi_L^*)$ and the $^3(\pi_H\pi_L^*)$ states. On the other

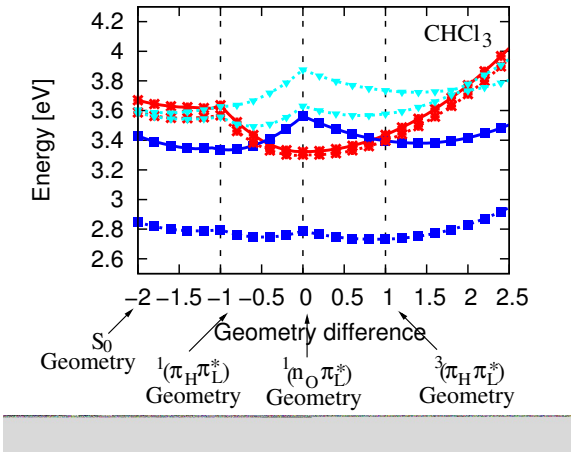

Fig. 6 DFT/MRCI excitation energy profiles in $CHCl_3$

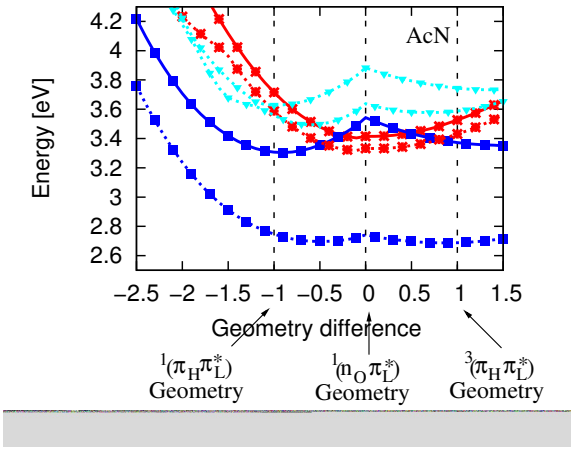

Fig. 7 DFT/MRCI excitation energy profiles in AcN

hand, the same effect leads to a diminuition of the energy gap between the $^{1,3}(n_O\pi_L^*)$ and the $^1(\pi_H\pi_L^*)$ states, hinting at some interesting photophysics going on.

The rate constant for the fluorescence decay process is about the same as in vacuum, namely, $6.1\times10^7 s^{-1}$. A comparison of the LIPs depicted in Figs.4 and 7 shows clearly the effect of polarity on the PE curves of the various electronic states. Due to the polarity of the solvent, the PES of the $(n_O\pi_L^*)$ states are blue shifted as compared to the vacuum and as a result, the $^1(\pi_H\pi_L^*)$ now lies below the $^1(n_O\pi_L^*)$ state at its adiabatic minimum. However, the PES of the two singlet states intersect each other at about 0.12 eV above the adiabatic minimum of the bright state. Furthermore, the adiabatic minimum of the $^1(n_O\pi_L^*)$ state (at 3.39 eV) is nearly isoenergetic with that of the $^1(\pi_H\pi_L^*)$ (at 3.30 eV), leading us to expect the IC between the two states to play a significant role in depleting the population of the latter state.

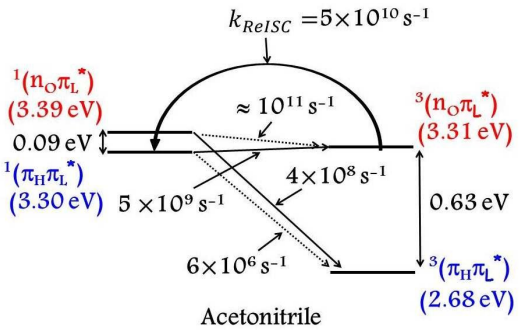

Fig. 8 The feasible ISC channels in photoexcited AC in AcN

Moving along the LIP on the $^1(\pi_H\pi_L^*)$ PES, another crossing is encountered, this time with the $^3(n_O\pi_L^*)$ state. The PES of the bright and this triplet state cross each other around 3.36 eV, only 0.06 eV above the adiabatic minimum of the $^1(\pi_H\pi_L^*)$ state. The rate constant for the population transfer via El-Sayed allowed ISC process, $^1(\pi_H\pi_L^*) \rightsquigarrow ^3(n_O\pi_L^*)$, is computed as $5\times10^9 s^{-1}$. The adiabatic minima of the involved states being isoenergetic (see Fig.7), with the minimum of the triplet state lying marginally above that of the singlet state, and considering the fact that under such circumstances the vibrational density of states (VDOS) is not very large, one may not be surprised that this rate constant is about two orders of magnitude smaller than that for the same process in vacuum. Vibronic coupling effects may not be left out when the states with $(n_O\pi_L^*)$ and $(\pi_H\pi_L^*)$ character are in such close vicinity. In fact the largest ISC rate constant, $k_{ISC} \approx 10^{11} s^{-1}$, has been determined for the El-Sayed forbidden $^1(n_O\pi_L^*) \rightsquigarrow ^3(n_O\pi_L^*)$ ISC process. The direct $^1(n_O\pi_L^*) \rightsquigarrow ^3(\pi_H\pi_L^*)$ and the vibronically activated $^1(\pi_H\pi_L^*) \rightsquigarrow ^3(\pi_H\pi_L^*)$ ISC channels are negligible, being at least an order of magnitude smaller than the other radiationless deactivation channels (see Fig.8). Thus, we may summarize that the bright state depopulates via IC to $^1(n_O\pi_L^*)$ and ISC to $^3(n_O\pi_L^*)$. The $^3(n_O\pi_L^*)$ is also populated through vibronically promoted ISC out of the $^1(n_O\pi_L^*)$ state. This will then be followed by IC from the $^3(n_O\pi_L^*)$ to the lowest-lying $^3(\pi_H\pi_L^*)$ state.

It may appear that radiative decay plays no role in the photophysics, k_f being a few orders of magnitude smaller than the rate constants for the radiationless transitions. However, the near isoenergeticity of the $^1(\pi_H\pi_L^*)$ and $^3(n_O\pi_L^*)$ states leads us to draw parallels with the case of TX in methanol.[8,9] The back population of $^1(\pi_H\pi_L^*)$ via reverse ISC (ReISC) from the $^3(n_O\pi_L^*)$ is expected. A rate constant of $k_{ReISC} = 5\times10^{10} s^{-1}$ is determined computationally for the $^3(n_O\pi_L^*) \rightsquigarrow ^1(\pi_H\pi_L^*)$ process. This de- and back population of the bright state allows us to predict that delayed fluorescence could be observed for AC in AcN. In the long run, however, the $^3(\pi_H\pi_L^*)$ state would be populated via IC from the $^3(n_O\pi_L^*)$ state. The $^3(\pi_H\pi_L^*)$ state would be a long-lived state, as

it does not couple strongly to the ground state. Such long-lived triplet states make AC a good triplet sensitizer.

With regard to the role of AC in triplet-triplet annihilation upconversion, we can safely consider AC as a good candidate in vacuum/apolar or slightly polar media. AcN, on the other hand, may already be too polar, though a stable $^3(\pi_H\pi_L^*)$ formation would facilitate the triplet sensitizer function of AC.

Methanol. As already mentioned above, in our former works with related molecules we have found that not only the polarity but also the hydrogen bonding capacity of the solvent plays a decisive role in the photophysics of the solute. The energy landscape changes in MeOH primarily due to the enhancement of the blue shift experienced by the $(n_O\pi_L^*)$ states by about 0.2 eV.

As implied by the course of the PES (Fig.10) and the relative positions of the adiabatic minima of the excited states (Table2), radiationless deactivation of the $^1(\pi_H\pi_L^*)$ state are no longer feasible. This is corroborated by the absence of a crossing between the $^1(\pi_H\pi_L^*)$ state with other electronic states along the LIP (see Fig.10). Hence, we conclude, that after photoexcitation, the molecule should relax predominantly via fluorescence. The computed rate constant for this process $k_f = 8.4\times10^7$ s^{-1} compares very well with that reported for AC in ethanol, $k_f = 7.4\times10^7$ s^{-1}.[28]

Mory et al. measured the S_1-S_n absorption of AC in ethanol and found a maximum at about 698 nm.[29] Our calculations show this maximum to be at 721 nm, in excellent agreement with the experimental results. The estimated adiabatic energy of the $^3(\pi_H\pi_L^*)$ at 2.53 eV agrees well with that reported by Shcherbo et al. for AC in ethanol, namely, 2.61 eV.[30] In the literature, we found a work by Miyashita et al. who measured the triplet-triplet absorption of AC in ethanol at room temperature.[31] They report two absorption bands at 571 nm and 357 nm, respectively. We calculated the T-T_n absorption spectrum in MeOH (comparable to ethanol) at the $T(\pi_H\pi_L^*)$ minimum (see Fig.9). The stick spectrum has been convoluted using Gaussian functions with a fwhm (full width at half maximum) of 50 nm. The calculations reproduce the experimental results nearly perfectly (compare Fig.9 in this work and Fig.6 in Ref.23). The strongest absorption at 546 nm (571 nm in experiment) in the present work is allocated to the $\pi_L^* \rightarrow \pi_{L+2}^*$ transition. In the 420-350 nm (experimental value 357 nm) region, we find three transitions contributing to the small hump. Since the experiments were performed at room temperature, perhaps the individual lines could not be identified.

Boużyk et al. presented a theoretical study of the electronic absorption and emission of AC.[26] Among other solvents, they have also carried out calculations for AC in AcN using the PM3/CI method. However, they compared these reults for the polar, nonprotic solvent with that of the results obtained by Miyashita et al. in ethanol which is a polar, protic solvent. We have already emphasised how strongly the proticity of the solvent affects the

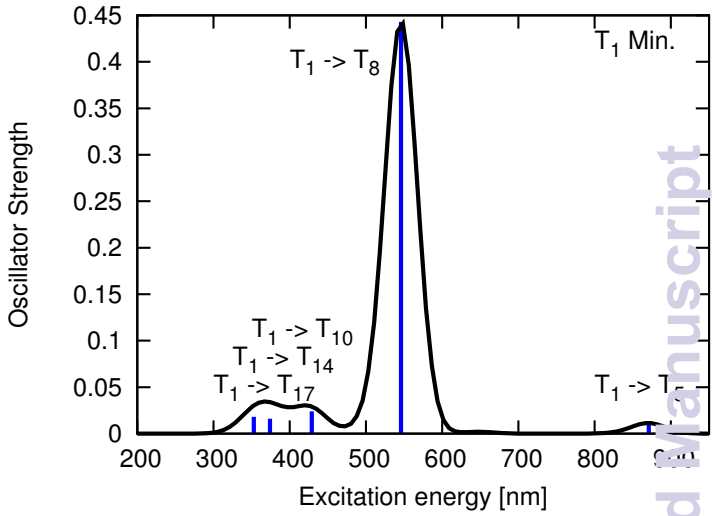

Fig. 9 T_1-T_n absorption spectrum in MeOH at the $T(\pi_H\pi_L^*)$ minimum.

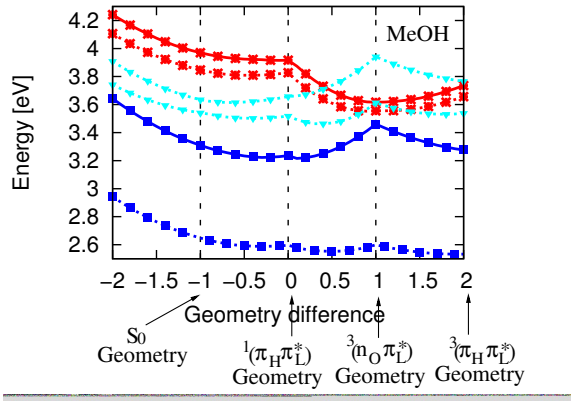

Fig. 10 DFT/MRCI excitation energy profiles in MeOH.

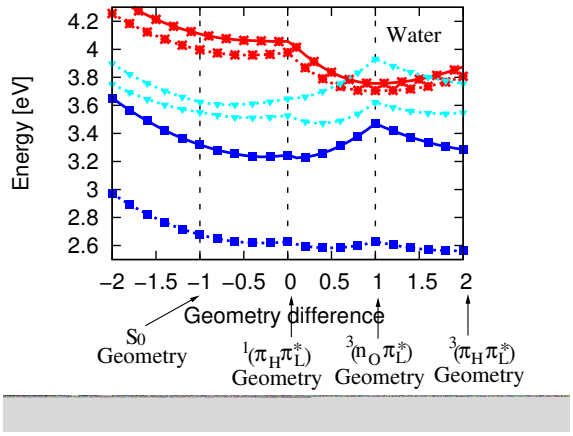

Fig. 11 DFT/MRCI excitation energy profiles in water.

energy landscape. Hence, the good agreement with experiment achieved by Boużyk et al. is surprising. Since their theoretical results in AcN have been scaled in order to achieve a better fit with the experimental spectra, we have refrained from comparing these findings with our results for AcN.

As implied by the course of the PES (Fig.10) and the relative positions of the adiabatic minima of the excited states (Table2), radiationless deactivation of the $^1(\pi_H\pi_L^*)$ state is no longer feasible. This is corroborated by the absence of crossings between the $^1(\pi_H\pi_L^*)$ state with other electronic states along the LIP (see Fig.10). Hence, we conclude, that after photoexcitation, the molecule should relax predominantly via fluorescence. The computed rate constant for this process $k_f = 8.4 \times 10^7$ s^{-1} compares very well with that reported for AC in ethanol, $k_f = 7.4 \times 10^7$ s^{-1}.[28]

Water. Fluorescence to the ground state out of the $^1(\pi_H\pi_L^*)$ state should also dominate the photophysics in water. The blue shifts being even more pronounced than in MeOH, a radiationless relaxation channel is not feasible. This explains why AC finds application as a fluorescence marker in biological systems.

Mitsui et al. have discussed the effect of microscopic solvation with water on the photophysics of AC.[24] From their analysis they conclude that the ISC in water between the bright singlet state and the triplet $(n\pi^*)$ states is no longer feasible as the two states experience oppsite energy shifts due to the formation of H-bonds.

The LIPs between the minima of the relevant electronic states in water (see Fig.11) no longer show any crossings that would indicate facilitated radiationless relaxation channels for the photoexcited bright singlet state. Hence, fluorescence should be the dominant decay channel after photoexcitation with a calculated rate constant of $k_f = 6.2 \times 10^7$ s^{-1}. González-Blanco et al. have reported a single exponential decay of AC in water with a time constant of 14.9 ns, which is in excellent agreement with our k_f value.[32]

5 Conclusion

Comparing the series of molecules X, TX and AC, we find a smooth variation in their photophysical behaviour. Whereas X fluoresces in the highly polar-protic solvent water, AC shows this behaviour already in the comparatively less polar-aprotic solvent AcN. In X, the adiabatic minima of the bright $^1(\pi_H\pi_L^*)$ and the dark $^1(n_O\pi_L^*)$ states lie about 0.71 eV apart in vacuum, whereas in AC this difference is only 0.30 eV. Hence, the polarity of AcN is enough to push the dark $n_O\pi_L^*$ state above the bright $^1(\pi_H\pi_L^*)$ states in AC, making them unavailable for radiationless relaxation purposes. Thus, AC may relax via radiative channel in AcN.

A detailed quantum chemical analysis of the photophyics of AC in the isolated and solvated states has been presented in this work. The minima and properties of the ground and relevant excited states have been determined using high level electronic structure methods. The effect of solvent polarity and specific bond formation on the photoexcitation processes has been studied in detail. Analog to what we found for related molecules TX and X, the photophysics is controlled by the rather large blue shift experienced by the $n_O\pi_L^*$ states. The red shift undergone by the electronic states with $^1(\pi_H\pi_L^*)$ is at least twice as small. The higher-lying multiconfigurational $\pi\pi^*$ states are hardly affected by the surrounding medium.

These energy shifts cause the PES of the various electronic states to cross each other. The LIPs between the minima of the states of interest have been calculated in order to get a qualitative picture of the feasible decay processes that may occur after the initial photoexcitation. Besides, computations were carried out to determine the rate constants of the radiative and radiationless processes, wherever possible and plausible.

The rate constant for the decay via fluorescence from the $^1(\pi_H\pi_L^*)$ state is nearly the same in all the cases. In vacuum *and* $CHCl_3$ *the radiative process* is quenched by the much faster radiationless IC and ISC *channels*. Going on to the polar medium of AcN, we still find the IC and ISC processes to be predominant. However, there is an important difference as compared to the *previous cases*. In AcN we predict that the photoexcited molecule may also show delayed fluorescence. The delayed fluorescence in AcN is possible due to the isoenergeticity of the adiabatic minima of the $^1(\pi_H\pi_L^*)$ and $^3(n_O\pi_L^*)$. Such a constellation of energetic layout facilitates the process of reverse ISC from the triplet to the singlet state. Hence, at a larger timescale, fluorescence should be observed in AcN. The hydrogen bond formation occuring in the polar, protic solvents MeOH and water further enhances the energy gap between the $\pi_H\pi_L^*$ and $n_O\pi_L^*$ states. This leads to the non availability of the radiationless decay channels, since the states that could be suitable candidates are not reachable due to the

large adiabatic energy differences. Hence, in polar, protic solvents the main decay channel is expected to be fluorescence to the ground state after photoexcitation.

AC is an unusual species, in that it may act as a triplet sensitizer (photorelaxation leads to triplet formation) or as a fluorescence marker (photorelaxation does not lead to triplet formation but to fluorescence) depending upon the medium surrounding it. Hence, the analysis of the photophysics as presented in this work may be employed as a guide to tune the surrounding medium in such a way, so as to turn on either the triplet sensitizer or the fluorescent marker properties of AC.

6 Acknowledgements

Financial support by the Deutsche Forschungsgemeinschaft through grant MA1051/12-1 is gratefully acknowledged. We thank Prof. Peter Gilch (Düsseldorf) for helpful discussions.

References

1 G. Chloewiński, K. Dzierzbicka and A. M. Kołodziejczyk, *Pharmacological Reports*, 2011, **63**, 305–336.

2 J. Zhao, S. Ji and H. Guo, *RSC Adv.*, 2011, **1**, 937–950.

3 A. Dadabhoy, S. Faulkner and P. G. Sammes, *J. Chem. Soc. Perkin Trans.*, 2000, **2**, 2359–2360.

4 Y. Hagiwara, T. Hasegawa, A. Shoji, M. Kuwahara, H. Ozaki and H. Sawai, *Bioorg. Med. Chem.*, 2008, **16**, 7013–7020.

5 K. D. Thériault, C. Radford, M. Parvez, B. Heyne and T. C. Sutherland, *Phys. Chem. Chem. Phys.*, 2015, **17**, 20903–20911.

6 V. Rai-Constapel, M. Etinski and C. M. Marian, *J. Phys. Chem. A*, 2013, **117**, 3935–3944.

7 V. Rai-Constapel, S. Salzmann and C. M. Marian, *J. Phys. Chem. A*, 2011, **115**, 8589–8596.

8 V. Rai-Constapel, T. Villnow, G. Ryseck, P. Gilch and C. M. Marian, *J. Phys. Chem. A*, 2014, **118**, 11708–11717.

9 T. Villnow, G. Ryseck, V. Rai-Constapel, C. M. Marian and P. Gilch, *J. Phys. Chem. A*, 2014, **118**, 11696–11707.

10 A. D. Becke, *J. Chem. Phys.*, 1993, **98**, 5648–5652.

11 C. Lee, W. Yang and R. G. Parr, *Phys. Rev. B*, 1988, **37**, 785.

12 A. Schäfer, C. Huber and R. Ahlrichs, *J. Chem. Phys.*, 1994, **100**, 5829.

13 *TURBOMOLE, a development of University of Karlsruhe and Forschungszentrum Karlsruhe GmbH, 1989-2007, TURBOMOLE GmbH, since 2007; available from* `http://www.turbomole.com`.

14 F. Furche and R. Ahlrichs, *J. Chem. Phys.*, 2002, **117**, 7433–7447.

15 J. Neugebauer, M. Reiher, C. Kind and B. A. Hess, *J. Comp. Chem.*, 2002, **23**, 895–910.

16 A. Klamt and G. Schüürmann, *J. Chem. Soc., Perkin Trans. 2*, 1993, **5**, 799–805.

17 A. Schäfer, A. Klamt, D. Sattel, J. C. W. Lohrenz and F. Eckert *Phys. Chem. Chem. Phys.*, 2000, **2**, 2187–2193.

18 S. Grimme and M. Waletzke, *J. Chem. Phys.*, 1999, **111**, 5645–5656.

19 J. Tomasi, B. Mennucci and R. Cammi, *Chem. Rev.*, 2005, **105** 2999–3094.

20 M. Kleinschmidt, J. Tatchen and C. M. Marian, *J. Comput Chem.*, 2002, **23**, 824–833.

21 M. Kleinschmidt and C. M. Marian, *Chem. Phys.*, 2005, **311** 71–79.

22 M. Etinski, J. Tatchen and C. M. Marian, *J. Chem. Phys.*, 2011 **134**, 154105–154114.

23 M. Etinski, V. Rai-Constapel and C. M. Marian, *J. Chem. Phys.*, 2014, **140**, 114104–1–14.

24 M. Mitsui, Y. Ohshima and O. Kajimoto, *J. Phys. Chem.A* 2000, **104**, 8660–8670.

25 M. Siegmund and J. Bendig, *Z. Naturforsch.*, 1980, **35a** 1076–1086.

26 A. Boużyk, L. Jóźwiak, A. Y. Kolendo and J. Błażejowski, *Spec. Act. A*, 2003, **59**, 543–558.

27 M. Mitsui and Y. Ohshima, *J. Phys. Chem. A*, 2000, **104**, 8638–8648.

28 S. J. Strickler and R. A. Berg, *J. Chem. Phys.*, 1962, **37**, 814–822.

29 S. Mory, H.-J. Weigmann, A. Rosenfeld, M. Siegmund, R. Mitzner and J. Bendig, *Chem. Phys. Lett.*, 1985, **115**, 201–204.

30 S. Shcherbo, G. Val'kova and D. Shigorin, *Russ. J. Phys. Chem.*, 1981, **55**, 452–455.

31 Y. Miyashita, S. Niizuma, H. Kokubun and M. Koizumi, *Bull. Chem. Soc. Jpn.*, 1973, **46**, 3373–3377.

32 C. González-Blanco, M. Velázquez, S. M. Costa and P. Barreleiro, *J. Colloid Interface Sci.*, 1997, **189**, 43 – 50.